Intravoxel Incoherent Motion Diffusion-weighted MR Imaging for Monitoring the Immune Response of Immunogenic Chemotherapy

Junjiao Hu
Jinan University First Affiliated Hospital
Xin Yu
Jinan University First Affiliated Hospital
Peidi Yin
Jinan University First Affiliated Hospital
Lin Qiu
Jinan University First Affiliated Hospital
Bin Du
Tongji University School of Medicine
Xiangran Cai (caixran@jnu.edu.cn)
Jinan University First Affiliated Hospital

Research

Keywords: Magnetic resonance imaging, Diffusion-weighted imaging, Intravoxel incoherent motion, metronomic chemotherapy, Immune response prediction

Posted Date: June 22nd, 2021

DOI: https://doi.org/10.21203/rs.3.rs-630224/v1

Abstract

Background: Traditional chemotherapeutic drugs have the potential to increase tumor cell immunogenicity by activating immunogenic cell death (ICD). The accumulation of preclinical and clinical evidence suggests that the success of neoadjuvant chemotherapy, immunogenic chemotherapy depends (at least in part) on their ability to stimulate anti-cancer immune responses. Although the pathological examination is the gold standard for detecting the antitumor immune response, it is invasive and cannot be performed repetitively. Hence, the aim of our study was to evaluate the predictive value of intravoxel incoherent motion (IVIM) diffusion-weighted imaging (DWI) in the quantitative assessment of conventional chemotherapy-activated immune responses in mouse tumor models and clinics.

Methods: A total of 19 subcutaneous tumor-bearing mice were randomly divided into treated and control groups. Both groups had orderly IVIM DWI examinations before and on days 6 and 12 after the administration of cyclophosphamide (CPA) or saline. The expressions of immune-related genes in the tumor were measured by qPCR or detected by immunohistochemical assay. In addition, six patients with breast cancer requiring neoadjuvant chemotherapy also underwent functional MRI examinations. The primary statistical analysis methods were the Wilcoxon test of variance, correlation analysis, and the Kruskal-Wallis H test.

Results: The tumoral pseudodiffusion coefficient (D*), the perfusion fraction (*f*), and the blood flow-related parameter (fD*) of the treatment group showed a trend that significantly decreased on day 6. Then, these values increased on day 12, while they displayed the opposite tendency in the control group. Compared with the control group, a strong induction of the expression of the immune responses in the CPA treatment group was observed on day 12. Additionally, the changes in functional MRI parameters in the six patients with breast cancer after neoadjuvant chemotherapy showed similar trends to those in the tumor-bearing mice in the CPA treatment group.

Conclusions: The immune response induced by immunogenic chemotherapy could be effectively evaluated using IVIM-DWI. The D and D* values could be potential, sensitive imaging markers for identifying the antitumor immune response initiated by immunogenic chemotherapy.

Background

Conventional cytotoxic cancer chemotherapy is often immunosuppressive and associated with drug resistance and tumor regrowth(1–3). However, traditional chemotherapeutic drugs, including doxorubicin, mitoxantrone, and cyclophosphamide (CPA), have the potential to increase tumor cell immunogenicity by activating immunogenic cell death (ICD), an immunostimulatory form of cell death that activates innate immune responses and elicits a tumor-specific adaptive immune response(4–6). Neoadjuvant chemotherapy or primary systemic therapy is considered the standard treatment for locally advanced breast cancer. The accumulation of preclinical and clinical evidence indicates that the success of anthracycline-based neoadjuvant chemotherapy for breast cancer depends (at least in part) on their

ability to stimulate anticancer immune responses(7–9). High levels of tumor-infiltrating lymphocytes (TILs) are predictive of complete pathological response after neoadjuvant chemotherapy in certain breast cancers.

Immunogenic chemotherapy is a regimen characterized by regular and frequent chemotherapeutic drug doses that maintain a low but active antitumor immune response during prolonged periods without significant toxicity. Immunogenic chemotherapy can inhibit tumor angiogenesis, stimulate the antitumor immune response, and induce tumor dormancy(10). A study revealed that medium-dose, intermittent chemotherapy (MEDIC) of CPA could induce complete immune cell-dependent regression of GL261 tumors implanted in immune-competent C57BL/6 mice in a GL261(B6) tumor model and activate long-term tumor-specific immunity(11). Specifically, MEDIC chemotherapy of CPA could stimulate the production and release of type-I interferons and lead to the robust activation of downstream gene targets, including Mx1 and Cxcl10 (11). These tumor-associated gene responses are linked to innate immune cell recruitment and tumor regression.

In clinical practice, monitoring the antitumor immune response is critical and may convey robust predictive or prognostic indications(12, 13). However, clinical challenges remain in identifying those patients most likely to respond and to a accurately monitor the clinical response when patients receive antitumor treatment. Although the pathological examination is the gold standard for detecting the antitumor immune response, it is invasive. This examination cannot be performed repetitively because of the potential risk of infection and metastasis. Therefore, it is worth having a reliable and noninvasive biomarker to identify and monitor the antitumor immune response.

Intravoxel incoherent motion diffusion-weighted imaging (IVIM-DWI), a promising functional MRI imaging technique, could evaluate imaging features of the tumor and assess the therapeutic efficacy after radio/chemotherapy in many tumors(14–17). However, there are still no studies that assess the immune response induced by anti-neoplastic agents using IVIM-DWI. Hence, this study aims to investigate the utility of IVIM DWI in detecting the immune response induced by MEDIC chemotherapy of CPA in a GL261 mouse glioma model and induced by neoadjuvant chemotherapy in patients with breast cancer.

Material And Methods

Tumor Cell lines, Mouse Tumors, and Treatments

The GL261 murine glioblastoma cells (DSMZ, Germany) were cultured in Dulbecco's modified Eagle medium (DMEM) supplemented with 10% fetal bovine serum (FBS) and 1% penicillin/streptomycin (Gibco, USA). Six-week-old male C57BL/6 (B6) mice weighing between 20 and 23 g (Beijing, China) were housed in a specific pathogen-free environment maintained at 18-22 °C, with a relative humidity of 60–70% and 12 h of light daily. After a 1-week adaptation period, GL261 glioma cells (5×10^6) were implanted by subcutaneous injection into the posterior flanks in 0.2-mL serum-free RPMI per site using a U-100 insulin syringe and 28.5 gauge needles (BD Biosciences, Cat.# 329461). Mouse body weights were

measured at least twice a week and normalized in the same manner. The tumors were permitted to grow to 200 mm^3 before treatment (approximately two weeks after implantation). To evaluate the therapeutic response, the tumor area (length £ width) was measured twice weekly using Vernier calipers (VWR International, Cat.# 62379-531), and the tumor volume was calculated as Vol D $(\pi/6)*(L*W)^{3/2}$. The mice in the treated group (n = 14) were intraperitoneally administered CPA monohydrate (Cat. # C0768, Sigma-Aldrich, St. Louis, MO) every 6 days at a dose of 140 mg/kg-body weight per injection (CPA-140); CPA was injected twice during the entire experiment. The control group (n=5) received an intraperitoneal injection of saline at the same dose. C57BL/6 mice bearing GL261 gliomas underwent IVIM DWI at baseline and after 6 and 12 days of treatment with metronomic cyclophosphamide.

MR imaging

All the experimental mice were anesthetized by intraperitoneal injection of 0.1% pentobarbital sodium before MR image acquisition. MR imaging was performed immediately before treatment (day 0, baseline) and on days 6 and 12 after CPA treatment for both the processed and control groups.

An MR imaging (MRI) was performed on a clinical 3.0-T MRI system (Signa HDxt, GE Medical System, Milwaukee, WI, USA) with a custom-built 4-channel receiver coil with a 3 cm inner diameter (Shenzhen Teshen Electric Co., Ltd., Shengzhen, China). The mouse was imaged in the prone position, the head was advanced, and the tumor center was placed between the center of the coil and the magnet. To reduce motion artifacts at the interface between the tumor and the air, a thin piece of pork was placed over the surface of the tumor.

After routine localization images were obtained, transverse T2-weighted fast spin-echo images (repetition time msec/echo time msec, 3000/68; section thickness, 1.6 mm; matrix, 288× 288) and T1-weighted images using a gradient echo sequence (625.0/9.4; section thickness, 1.6 mm; matrix, 288× 288) were acquired. Subsequently, the IVIM-DWI sequence was generated using single-shot echo-planar imaging with 12 b-values of 0, 20, 50, 100, 150, 200, 400, 600, 800, 1200, 1600, and 2000 sec/mm2. The following parameters were used for this sequence: TR/TE, 3000 ms/102.4 ms; flip angle, 90°; matrix, 128 × 64; field of view, 10 × 10 cm; section thickness, 2.9 mm; NEX, 4; and total scanning time, 6 mins and 35 s.

Imaging analysis of IVIM parametric map and quantitative measurement

Based on the biexponential fitting to the IVIM model, the relationship between the signal variation and b value can be described by the following equation(18):

$SI/S0=f\ exp(-bD*)+(1-f)exp(-bD)$. where f is the perfusion fraction, D is the molecular diffusion coefficient, and D* is perfusion-related diffusion. All IVIM images were transferred to a dedicated postprocessing workstation (ADW4.3, GE Healthcare) for quantitative analysis. The mean values of all IVIM parameters were measured independently by two radiologists (Cheng ZY and Feng YZ) with 5 years of experience in MRI. After identifying the solid part of the tumor on conventional T2WI, regions of interest (ROIs) were manually drawn on the center slice for each tumor on the axial DWI image with a b

value of 2000 s/mm2. All ROIs should cover as much of the solid part of the tumor as possible and avoid the hemorrhagic, cystic, and necrotic areas. The IVIM parameter maps were generated automatically by the MADC program, and the average of three ROI values was used as a representative parametric value.

Histological assessment and Quantitative Real-time PCR

After the lasting MRI scanning, all the experimental mice were sacrificed by cervical dislocation with deep anesthesia by using intraperitoneal injection with pentobarbital sodium.

The tumors were excised and frozen in liquid nitrogen for RNA isolation, tissue cryosectioning, and immunohistochemistry. A portion of the tumor was used for RNA isolation. Another portion was fixed in 4% paraformaldehyde overnight, dehydrated in 70% ethanol, and subsequently embedded in paraffin for tissue cryosectioning and immunohistochemistry. Murine glioblastoma cells were harvested from 6-well plates with TRIzol Reagent (Life, USA), and tumor tissue homogenate was obtained with a homogenizer (Kinematica, Switzerland). *In vitro*, cells were seeded in 6-well plates and treated with 20 μg/mL free poly(I:C), Au:poly(I:C), or 1 mM TMZ for 24 h. RNA was extracted according to the TRIzol RNA isolation protocol, cDNA was synthesized with a reverse transcriptase kit. Real-time PCR was performed with an SYBR Premix Ex Taq Kit (Takara, Japan) in a CFX96 Touch Real-Time PCR System (Bio-Rad, USA). The cDNA was denatured at 95 °C for 30 s and amplified at 95 °C for 5 s and 60 °C for 25 s (40 cycles).

Study Population

We enrolled six consecutive patients who had been scheduled for NAC from June 2020 to July 2020. All patients met the following criteria: (1) unilateral invasive ductal carcinoma confirmed by needle biopsy before NAC; (2) routine MRI and IVIM-DWI scans were performed before NAC, after cycle one (in the first three days of cycle two), and after cycle two (in the first three days of cycle two); (3) no surgery, chemo/radiotherapy, hormone therapy or any other treatment before the first MR examination; (4) no evidence of distant metastases before NAC; and (5) surgery at our hospital within three weeks after the completion of NAC.

Chemotherapy regimens

The Chemotherapy regiment was composed of a TAC regimen (docetaxel, cyclophosphamide, pirarubicin) for 4 patients: and another TAC regimen (docetaxel, epirubicin, cyclophosphamide) for 2 patients.

Imaging Technique

MR imaging (MRI) was performed on a clinical 3.0-T MRI system (Signa HDxt, GE Medical System, Milwaukee, WI, USA) with a 4-channel breast coil. The subject was asked to lie in the prone position, with the breasts naturally falling in the coil.

Horizontal T2 fat suppression images (repetition time msec/echo time msec, 3570/72; section thickness, 5.0 mm; matrix, 256× 230) and horizontal T1 fat suppression images (repetition time msec/echo time msec, 169.0/92.61; section thickness, 4.0 mm; matrix, 448×380) were acquired.

The IVIM-DWI sequence was generated using single-shot echo-planar imaging with 12 b-values of 0, 20, 50, 100, 150, 200, 400, 600, 800, 1200, 1600, and 2000 sec/mm2. The following parameters were used for this sequence: TR/TE, 6400 ms/63.0 ms; flip angle, 90°; matrix, 192 × 192; field of view, 340 mm ×136 mm; section thickness, 5.0 mm; NEX, 4. The steps for imaging analysis and quantitative measurement of IVIM parameter maps were the same as those described above.

Statistical analysis

The SPSS 16.0 software (IBM Corporation, Chicago, IL, USA) and GraphPad Prism 7.01 (GraphPad Software Inc., San Diego, CA) were utilized to perform statistical tests and plot line charts. The quantitative results are expressed as medians and ranges.

For the comparison between the control and treated groups in glioma-bearing mice, the Wilcoxon rank-sum test was used to analyze the median values of IVIM-DWI parameters and all histopathological indices of the gliomas in C57BL/6 mice. The Mann-Whitney test was used to analyze the relative changes in IVIM-DWI values. The relative serial changes in IVIM-derived parameters of the tumors at each time point were evaluated by using the Friedman test in the treated group. The reproducibility of IVIM-DWI measurements of the tumors was analyzed by repeating the IVIM DWI sequence at 6-day intervals for five randomly selected experimental mice from the control group, and the coefficients of variation (CVs) were calculated. According to previous studies, CVs below or equal to 10%, 11%–24%, and greater than or equal to 25% represent good, moderate, and poor reproducibility, respectively(19). Spearman's rank correlation test was performed for correlations between histological features and the corresponding IVIM-DWI parameters. The Kruskal-Wallis test was used to analyze changes in the IVIM-DWI parametric values in breast cancer patients receiving neoadjuvant chemotherapy. An $r \geq 0.8$ was considered highly correlated, whereas $r < 0.8$ and $r \geq 0.5$ were considered mildly correlated. A P value < 0.05 was considered statistically significant.

Results

Effect of CPA Treatment on Tumor Growth

MEDIC CPA treatment for 12 days effectively inhibited the tumor growth of GL261 gliomas (Fig. 1). As shown in Fig. 1, the tumor volume of the treated group began to decrease on day 6 after CPA treatment, while that of the control group continued to increase. The tumor volume in the treated group was significantly lower than that in the control group on the 12th day ($P < 0.001$).

Reproducibility of IVIM-DWI Parameters

The tumoral D value in the control group demonstrated good reproducibility, with CVs of 7%. The D*, f, and fD* values showed moderate reproducibility, with CVs of 14.5%, 13.7%, and 15%, respectively.

IVIM-DWI parametric changes of tumors in the treated and control groups over time and the comparison between the two groups

In the treated group, the tumoral D*, f, and fD* values significantly decreased on day 6 compared with those at baseline and then increased to near baseline levels on day 12. However, those values showed the opposite trend in the control group, with a significant rise on day 6 and a reduction on day 12. The tumoral D values in the treated group demonstrated significantly consistent growth from baseline to day 12 after CPA treatment. In contrast, those in the control group gradually decreased (Table 1).

At baseline, there was no significant difference in any IVIM-DWI parameters between the control and treated groups. The tumoral D values in the treated group were significantly greater than those in the control group on both days 6 and 12 (P<0.005). In contrast, the D*, f, and fD* values in the treated group were significantly lower than those in the control group at the same time points (P<0.005) (Fig. 2-3).

Immune Cell Recruitment and Expression in the two groups

MEDIC CPA treatment-induced regression and immune cell infiltration in GL261 gliomas. Immune cell recruitment and expression in the CPA-treatment group were significantly higher than those in the control group on day 12. A massive increase in cytotoxic T-cells (CD8a) and the expression of type-I interferons were observed in the CPA group. Tumor regression was associated with a significant increase in immune cell infiltration, as revealed by the marker gene analysis in the completely excised GL261 tumors on day 12. Moreover, strong induction of the ISGs *Mx1* and *Cxcl10* was also observed (fig. 4-5).

Correlations of pathological examination or immune Cell Recruitment and Expression with IVIM-DWI Parameters

Our results revealed that the D value showed a positive correlation with the Ifnb1-, CD8a-, *Mx1*-, *Cxcl10*-, and TUNEL-positive staining rates (r =0.868, 0.864, 0.874, 0.885, and 0.858, respectively, P<0.0001) and a negative correlation with the Ki-67 index (r=-0.904, P<0.0001). The D* value showed a positive correlation with the CD31-positive staining rate (r=0.729, P<0.01).

IVIM-DWI Parametric changes in tumors in breast cancer patients with different cycles of neoadjuvant chemotherapy

Changes in IVIM-DWI parameters in the six breast cancer patients treated with neoadjuvant chemotherapy showed similar results to those in the tumor-bearing mice in the treatment group (Table 2). The tumoral D*, f, and fD* values gradually decreased with statistically significant differences. However, the tumoral D values demonstrated significantly consistent growth from cycle 1 to cycle 2 after neoadjuvant chemotherapy (fig. 6-7).The D value showed a positive correlation with CD8a (r =0.631, P =0.028) and a negative correlation with CD31 (r =-0.869, P =0.000) or Ki67 (r =-0.733, P

=0.007). Positive correlations were found between the D*, f, and fD* values and CD31 (r =0.776, P =0.003, r =0.634, P =0.027, and r =0.603, P =0.038, respectively) or *Ki67 (*r =0.771, P =0.003, r =0.881, P =0.000, and r =0.857, P =0.000, respectively), whereas negative correlations were displayed between those parametric values and CD8a (r =-0.675, P =0.016, r =-0.785, P =0.002, and r =-0.757, P =0.004, respectively).

Discussion

MEDIC of CPA is an immunogenic chemotherapy regimen that can inhibit tumor angiogenesis, stimulate the antitumor immune response, and induce tumor dormancy. This regimen is essential to monitor the antitumor immune response initiated by chemotherapy in clinical practice because they may convey a robust predictive or prognostic indication. IVIM-DWI is a valuable technique used in rating microcirculation perfusion and water diffusion. Our previous study showed that CPA treatment with a 6-day repeat to the MEDIC schedule induced complete, immune cell-dependent regression in cultured GL261 glioma(11). Therefore, this study aimed to investigate the utility of IVIM DWI in detecting the immune response induced by immunogenic chemotherapy.

We successfully built a mouse glioma model with induced antitumor immune responses, which involve three main steps (11, 20). First, MEDIC CPA treatment released immune signaling molecules, which activated CD8a. Then, the production of type-I interferons and robust induction of IFN-stimulated genes (ISGs) MX1 and CXCL10 finally led to ICD. The pathological findings on day 12 suggested an abundant immune cell infiltration within the glioma. Moreover, RT-qPCR analysis of immune cell marker genes, ISGs, and interferons demonstrated that immune response-related markers were expressed in abundance in the CPA group. These findings are indicative of a robust antitumor immune response within glioma. Tumor regression was associated with a significant increase in immune cell infiltration, which was also revealed by marker gene analysis in a completely excised GL261 tumor on day 12.

In the current study, the IVIM-DWI was used to monitor the antitumor immune response in a mouse GL261 subcutaneous xenograft tumor model at three-time points before and after chemotherapy. The IVIM-DWI parametric values indicated restricted water molecule diffusion and increased perfusion in glioma after CPA treatment related to the antitumor immune responses induced by CPA. Our results showed a persistently increased D value of the tumor up to the 12th day after CPA treatment, indicating an increase in the water diffusivity (21, 22). Theoretically, low cellularity increases in D values, as low cellularity leads to decreased cell membrane density [20]. Intermittent application of medium-dose CPA will strongly induce an antitumor immune response and inhibit tumor growth[2], which could be the main course for lower cellularity. Following successful treatment, it is widely noted that the tumor ADC value will increase, reflecting a reduction in cellular density and water motion barriers (23). Similar to our results, Thoeny et al. (24) revealed that the first decreased D-value at the 1- and 6-hour follow-ups and then significantly increased D-value was attributed to increased tumor necrosis after vascular disrupting agent (VDA) treatment in a rat tumor model on day 2.

In contrast, perfusion-related IVIM parameters, including D*, f, and fD* values, dramatically fell on day 6 and then rose to near the baseline level on day 12 in the treated group. The initial decline in perfusion within the tumor was due primarily to the toxic effect of CPA on endothelial cells of tumors and its destroying vascular effect. The administration of CPA on a metronomic schedule(25, 26) can augment CPA cytotoxicity to tumor-associated endothelial cells (27, 28). Bocci et al. (29) revealed that the metronomic CPA protocol induced or upregulated thrombospondin-1, an endogenous angiogenesis inhibitor. The metronomic CPA regimen was also capable of potent and sustained suppression of mobilization from the bone marrow of endothelial cell progenitors and vasculogenesis(30). Additionally, CPAs can induce inflammatory immune factors that inhibit tumor angiogenesis and disrupt pre-existing tumor blood vessels, leading to decreased blood flow and ICD, followed by ischemic changes such as cellular edema and intratumoral necrosis. These could be just an explanation of drastically reduced perfusion parameters on day 6 after CPA treatment. Subsequently, angiogenesis around the tumor was reconstructed; thus, the peripherally viable tumoral tissue survived and regrew(31), which temporarily increased tumor perfusion; therefore, the D*, f, and f D* values increased on day 12. Overall, the inhibition and reconstruction of angiogenesis of the tumor contributed to the changes in D*, f, and f D* values within the tumor.

We observed the opposite trend over time in the control group, demonstrating a decrease in D and a significant increase in D*, f, and fD* values on day 6 compared to those values at baseline and then a decrease on day 12. The tumor blood vessels were rich and immature in the control group without CPA treatment, which initially increased perfusion. Later, the tumor cells continued to grow further and even grew faster than blood vessels. Thus, tumor cells are dense, while the blood supply is inadequate. Subsequently, hypoxia and ischemic necrosis of cells occur, which could assist in the subsequent reduction of microcirculation perfusion.

Perfusion and diffusion changes after CPA treatment revealed by the IVIM DWI can be explained by histologic changes. In our study, perfusion-related parameters D* were significantly correlated with CD31 on day 12. D* represents the flow velocity in the capillary network of the microcirculation and is related to tissue blood flow(32). CD31, otherwise known as a platelet-endothelial cell adhesion molecule, is generally expressed in vascular endothelial cells and used to assess tumor angiogenesis(33). A lower CD31 level means lower vascularity of the tumor, which would lead to a lower D* value. In addition, the early changes observed in perfusion-related parameters within the tumor in the treated group may be due to the rapid collapse of the tumor vasculature induced by CPA. This collapse may result in a decrease in blood flow velocity (D*), volume (f), and flow-related (fD*) parameters(32, 34, 35). Bocci(29) et al. showed that CD31 tended to decrease over time after CPA treatment, which would result in a decrease in D*.

Ki67 is a cell proliferation index that can accurately reflect the proliferation activity of cells(36). The higher the value is, the more active the cell proliferation is. TUNEL (terminal deoxynucleotidyl transferase nick-end labeling) is used to detect cell apoptosis(37). The diffusion-related parameter D was significantly correlated with Ki-67 and TUNEL on day 12. D is the pure diffusion of water molecules in the extracellular space, and the D value is related to the cell density. When the cell density increases and the

extracellular space shrinks, the movement of water molecules is restricted, and the D-value decreases (23, 38, 39). On the 12th day after CPA treatment, the D value increased due to increased apoptosis, decreased cell density, and increased extracellular space. A lower Ki-67 or higher apoptosis of the tumor would lead to a higher D value.

In addition, we found strong (or robust) induction of immune response expression in the CPA treatment group. The D value was positively correlated with Ifnb1, CD8a, Mx1, and Cxcl10 expression. The CPA's antitumor immune mechanism could account for this strong correlation between IVIM parameters and immune cell recruitment and expression. This finding may be related to the large production and release of Ifnb1 induced by CPA chemotherapy. Ifnb1 has a potent inhibitory effect on tumor cell proliferation and immune regulation. First, it promotes macrophages to swallow antibody-coated tumor cells, activates NK cells, and enhances their cytotoxicity. In addition, it can inhibit the proliferation of tumor cells (40) and promote tumor cell apoptosis.(41) These factors will cause necrosis and fibrosis in tumor cells, reduce their internal density, expand the extracellular space, and finally reduce the diffusion of water molecules. Thus, the IVIM DWI could be a sensitive and noninvasive predictor in monitoring the antitumor immune response.

In this animal experiment, we demonstrated the feasibility of the IVIM-DWI technique for monitoring the immunostimulatory effects of CPA treatment in tumor-bearing mice. However, whether preclinical observations of such changes in the IVIM-DWI parameters are consistent with clinical findings is controversial. Therefore, we collected imaging data from 2 cycles of 6 patients with locally advanced breast cancer who required neoadjuvant chemotherapy. By analyzing the results of the imaging parameters, these changes followed a similar trend as in the animal experiment. Neoadjuvant therapy (NAT) for cancer is any anticancer treatment provided before the main treatment (which is usually surgery), and thus constitutes a form of induction therapy(42). In breast cancer, neoadjuvant chemotherapy is the preferred treatment approach for locally advanced cancers with pathologic complete response(43). Chemotherapy has long been considered immune suppressive; however, there is growing evidence that the efficacy of chemotherapy involves not only cell-intrinsic cytotoxic effects but also relies on the activation of antitumor immune responses(2). Recently, a study confirmed that after neoadjuvant chemotherapy for breast cancer, just one cycle of treatment can induce an immune stimulatory microenvironment and upregulation of inflammatory signatures(44). This finding may explain why the IVIM-DWI parameters follow the same trend in animal experiments and clinical trials.

Several factors constrained this study. First, only three time points were set to evaluate the antitumor immune response induced by CPA treatment. The increased time points could provide additional information about the dynamic variation of tumoral IVIM-DWI parameters for monitoring the antitumor immune response induced by CPA. Second, we selected one ROI on one axial MR image of the tumor to measure the IVIM-DWI parameters at each time point. However, considering the three-dimensional structure of the tumors, measurement on cross-sectional images might be less representative of the entire tumor than volumetric measurements. In addition, the measure by using one ROI, including the whole tumor, may not sufficiently reveal the pixel-by-pixel changes in serial follow-ups. Third, we analyzed the

correlations between the IVIM-derived parameters and immune cell recruitment and expression on day 12, whereas the correlation was not assessed on day 6. Finally, we did not compare the usefulness of the IVIM-DWI with other imaging modalities, such as dynamic contrast-enhanced MR imaging, in monitoring the antitumor immune response.

In conclusion, this study demonstrates that MEDIC CPA treatment for 12 days can induce a robust antitumor immune response, which significantly blocks tumor growth in a glioma model. The IVIM-DWI parameters could predict serial pathophysiological changes in tumor perfusion and diffusion. The IVIM-DWI technique has the potential to distinguish immune responders from immune nonresponders. This technique is expected to become an antitumor immune response biomarker for the initial prediction of antitumor response to immune chemotherapy regimens.

Conclusion

IVIM DW imaging-derived parameters may be used for the quantitative assessment of treatment efficacy and the prediction of tumor immune response after metronomic chemotherapy for patients with cancers.

Abbreviations

CPA, cyclophosphamide; MEDIC, medium-dose intermittent chemotherapy; RT-qPCR, reverse transcription-quantitative polymerase chain reaction; IFN, interferon; ISG, IFN-stimulated gene; CV = coefficient of variation; D = true diffusion coefficient; D* = pseudodiffusion coefficient; DW = diffusion weighted; f = perfusion fraction; fD* = blood flow-related parameter; IVIM = intravoxel incoherent motion.

Declarations

Acknowledgements

Not applicable

Authors' contributions

JH carried out the studies, participated in collecting data, and drafted the manuscript. JH , XY, LQ, and PY performed the statistical analysis and participated in its design. XC and BD reviewed and helped to draft the manuscript. All authors read and approved the final manuscript.

Funding

Not applicable.

Availability of data and materials

All experimental data generated or analyzed in this study are included in this published article.

Ethics approval and consent to participate

The Animal Experimental Ethical Inspection committee approved this animal study of Jinan University. (Approval no. 2019330-01), and the experimental process strictly abided by the animal ethics regulations. All studies on human subjects and material were approved by the local ethics committee.

Consent for publication

Not applicable.

Competing interests

The authors declare that they have no competing interests.

References

1. Zitvogel L, Kepp O, Kroemer G. Immune parameters affecting the efficacy of chemotherapeutic regimens. Nat Rev Clin Oncol. 2011;8(3):151-60.
2. Galluzzi L, Buqué A, Kepp O, Zitvogel L, Kroemer G. Immunological Effects of Conventional Chemotherapy and Targeted Anticancer Agents. Cancer Cell. 2015;28(6):690-714.
3. Shurin MR, Naiditch H, Gutkin DW, Umansky V, Shurin GV. ChemoImmunoModulation: immune regulation by the antineoplastic chemotherapeutic agents. Curr Med Chem. 2012;19(12):1792-803.
4. Wu J, Waxman DJ. Immunogenic chemotherapy: Dose and schedule dependence and combination with immunotherapy. Cancer Lett. 2018;419:210-21.
5. Inoue H, Tani K. Multimodal immunogenic cancer cell death as a consequence of anticancer cytotoxic treatments. Cell Death Differ. 2014;21(1):39-49.
6. Wang Q, Ju X, Wang J, Fan Y, Ren M, Zhang H. Immunogenic cell death in anticancer chemotherapy and its impact on clinical studies. Cancer Lett. 2018;438:17-23.
7. Chen Q, Xia R, Zheng W, Zhang L, Li P, Sun X, et al. Metronomic paclitaxel improves the efficacy of PD-1 monoclonal antibodies in breast cancer by transforming the tumor immune microenvironment. Am J Transl Res. 2020;12(2):519-30.
8. Iribarren K, Buque A, Mondragon L, Xie W, Lévesque S, Pol J, et al. Anticancer effects of anti-CD47 immunotherapy in vivo. Oncoimmunology. 2019;8(3):1550619.
9. Zheng DW, Chen JL, Zhu JY, Rong L, Li B, Lei Q, et al. Highly Integrated Nano-Platform for Breaking the Barrier between Chemotherapy and Immunotherapy. Nano Lett. 2016;16(7):4341-7.
10. Kareva I, Waxman DJ, Lakka Klement G. Metronomic chemotherapy: An attractive alternative to maximum tolerated dose therapy that can activate anti-tumor immunity and minimize therapeutic resistance. Cancer Letters. 2015;358(2):100-6.
11. Du B, Waxman DJ. Medium dose intermittent cyclophosphamide induces immunogenic cell death and cancer cell autonomous type I interferon production in glioma models. Cancer Lett.

2020;470:170-80.
12. Ladoire S, Chaba K, Martins I, Sukkurwala AQ, Adjemian S, Michaud M, et al. Immunohistochemical detection of cytoplasmic LC3 puncta in human cancer specimens. Autophagy. 2012;8(8):1175-84.
13. Ladoire S, Hannani D, Vetizou M, Locher C, Aymeric L, Apetoh L, et al. Cell-death-associated molecular patterns as determinants of cancer immunogenicity. Antioxid Redox Signal. 2014;20(7):1098-116.
14. Zhou Y, Liu J, Liu C, Jia J, Li N, Xie L, et al. Intravoxel incoherent motion diffusion weighted MRI of cervical cancer - Correlated with tumor differentiation and perfusion. Magn Reson Imaging. 2016;34(8):1050-6.
15. Liang CY, Chen MD, Zhao XX, Yan CG, Mei YJ, Xu YK. Multiple mathematical models of diffusion-weighted magnetic resonance imaging combined with prognostic factors for assessing the response to neoadjuvant chemotherapy and radiation therapy in locally advanced rectal cancer. Eur J Radiol. 2019;110:249-55.
16. Song SE, Cho KR, Seo BK, Woo OH, Park KH, Son YH, et al. Intravoxel incoherent motion diffusion-weighted MRI of invasive breast cancer: Correlation with prognostic factors and kinetic features acquired with computer-aided diagnosis. J Magn Reson Imaging. 2019;49(1):118-30.
17. Zhu S, Wei Y, Gao F, Li L, Liu Y, Huang Z, et al. Esophageal carcinoma: Intravoxel incoherent motion diffusion-weighted MRI parameters and histopathological correlations. J Magn Reson Imaging. 2019;49(1):253-61.
18. Le Bihan D, Breton E, Lallemand D, Grenier P, Cabanis E, Laval-Jeantet M. MR imaging of intravoxel incoherent motions: application to diffusion and perfusion in neurologic disorders. Radiology. 1986;161(2):401-7.
19. Iellamo F, Legramante JM, Raimondi G, Castrucci F, Massaro M, Peruzzi G. Evaluation of reproducibility of spontaneous baroreflex sensitivity at rest and during laboratory tests. J Hypertens. 1996;14(9):1099-104.
20. Wu J, Waxman DJ. Metronomic cyclophosphamide eradicates large implanted GL261 gliomas by activating antitumor Cd8(+) T-cell responses and immune memory. Oncoimmunology. 2015;4(4):e1005521.
21. Dóczi T, Schwarcz A. Correlation of apparent diffusion coefficient and computed tomography density in acute ischemic stroke. Stroke. 2003;34(5):e17-e8.
22. Wang H, Marchal G, Ni Y. Multiparametric MRI biomarkers for measuring vascular disrupting effect on cancer. World J Radiol. 2011;3(1):1-16.
23. Pickles MD, Gibbs P, Lowry M, Turnbull LW. Diffusion changes precede size reduction in neoadjuvant treatment of breast cancer. Magn Reson Imaging. 2006;24(7):843-7.
24. Thoeny HC, De Keyzer F, Chen F, Ni Y, Landuyt W, Verbeken EK, et al. Diffusion-weighted MR imaging in monitoring the effect of a vascular targeting agent on rhabdomyosarcoma in rats. Radiology. 2005;234(3):756-64.

25. Hahnfeldt P, Hlatky L, Klement GL. Center of cancer systems biology second annual workshop--tumor metronomics: timing and dose level dynamics. Cancer Res. 2013;73(10):2949-54.
26. Pasquier E, Kavallaris, M. A. Metronomic chemotherapy: new rationale for new directions. Nature Reviews Clinical Oncology. 2010;7(82):455–65.
27. Pasquier E, Tuset M, Street J. Concentration- and schedule-dependent effects of chemotherapy on the angiogenic potential and drug sensitivity of vascular endothelial cells. Angiogenesis. 2013;16(2):373-86.
28. Emmenegger U, Man S, Shaked Y. A comparative analysis of low-dose metronomic cyclophosphamide reveals absent or low-grade toxicity on tissues highly sensitive to the toxic effects of maximum tolerated dose regimens. Cancer research. 2004;64(11):3994-4000.
29. Bocci G, Francia G, Man S, Lawler J, Kerbel RS. Thrombospondin 1, a mediator of the antiangiogenic effects of low-dose metronomic chemotherapy. Proceedings of the National Academy of Sciences of the United States of America. 2003;100(22):12917-22.
30. Bertolini F, Paul S, Mancuso P, Monestiroli S, Gobbi A, Shaked Y, et al. Maximum tolerable dose and low-dose metronomic chemotherapy have opposite effects on the mobilization and viability of circulating endothelial progenitor cells. Cancer research. 2003;63(15):4342-6.
31. Tagliamonte M, Petrizzo A, Napolitano M, Luciano A, Rea D, Barbieri A, et al. A novel multi-drug metronomic chemotherapy significantly delays tumor growth in mice. J Transl Med. 2016;14:58.
32. Le Bihan D. What can we see with IVIM MRI? NeuroImage. 2019;187:56-67.
33. Lertkiatmongkol P, Liao D, Mei H, Hu Y, Newman PJ. Endothelial functions of platelet/endothelial cell adhesion molecule-1 (CD31). Current opinion in hematology. 2016;23(3):253-9.
34. Le Bihan D. Intravoxel incoherent motion perfusion MR imaging: a wake-up call. Radiology. 2008;249(3):748-52.
35. Sigmund EE, Vivier PH, Sui D, Lamparello NA, Tantillo K, Mikheev A, et al. Intravoxel incoherent motion and diffusion-tensor imaging in renal tissue under hydration and furosemide flow challenges. Radiology. 2012;263(3):758-69.
36. Sun X, Kaufman PD. Ki-67: more than a proliferation marker. Chromosoma. 2018;127(2):175-86.
37. Kyrylkova K, Kyryachenko S, Leid M, Kioussi C. Detection of apoptosis by TUNEL assay. Methods in molecular biology (Clifton, NJ). 2012;887:41-7.
38. Dóczi T, Schwarcz A. Correlation of apparent diffusion coefficient and computed tomography density in acute ischemic stroke. Stroke. 2003;34(5):e17-8; author reply e-8.
39. Wang H, Marchal G, Ni Y. Multiparametric MRI biomarkers for measuring vascular disrupting effect on cancer. World journal of radiology. 2011;3(1):1-16.
40. Ferrantini M, Capone I, Belardelli F. Interferon-alpha and cancer: mechanisms of action and new perspectives of clinical use. Biochimie. 2007;89(6-7):884-93.
41. Thyrell L, Hjortsberg L, Arulampalam V, Panaretakis T, Uhles S, Dagnell M, et al. Interferon alpha-induced apoptosis in tumor cells is mediated through the phosphoinositide 3-kinase/mammalian

target of rapamycin signaling pathway. The Journal of biological chemistry. 2004;279(23):24152-62.
42. Untch M, Konecny GE, Paepke S, von Minckwitz G. Current and future role of neoadjuvant therapy for breast cancer. Breast. 2014;23(5):526-37.
43. Curigliano G, Burstein HJ, Winer EP, Gnant M, Dubsky P, Loibl S, et al. De-escalating and escalating treatments for early-stage breast cancer: the St. Gallen International Expert Consensus Conference on the Primary Therapy of Early Breast Cancer 2017. Ann Oncol. 2017;28(8):1700-12.
44. Park YH, Lal S, Lee JE, Choi YL, Wen J, Ram S, et al. Chemotherapy induces dynamic immune responses in breast cancers that impact treatment outcome. Nat Commun. 2020;11(1):6175.

Tables

Due to technical limitations, tables docx is only available as a download in the Supplemental Files section.

Figures

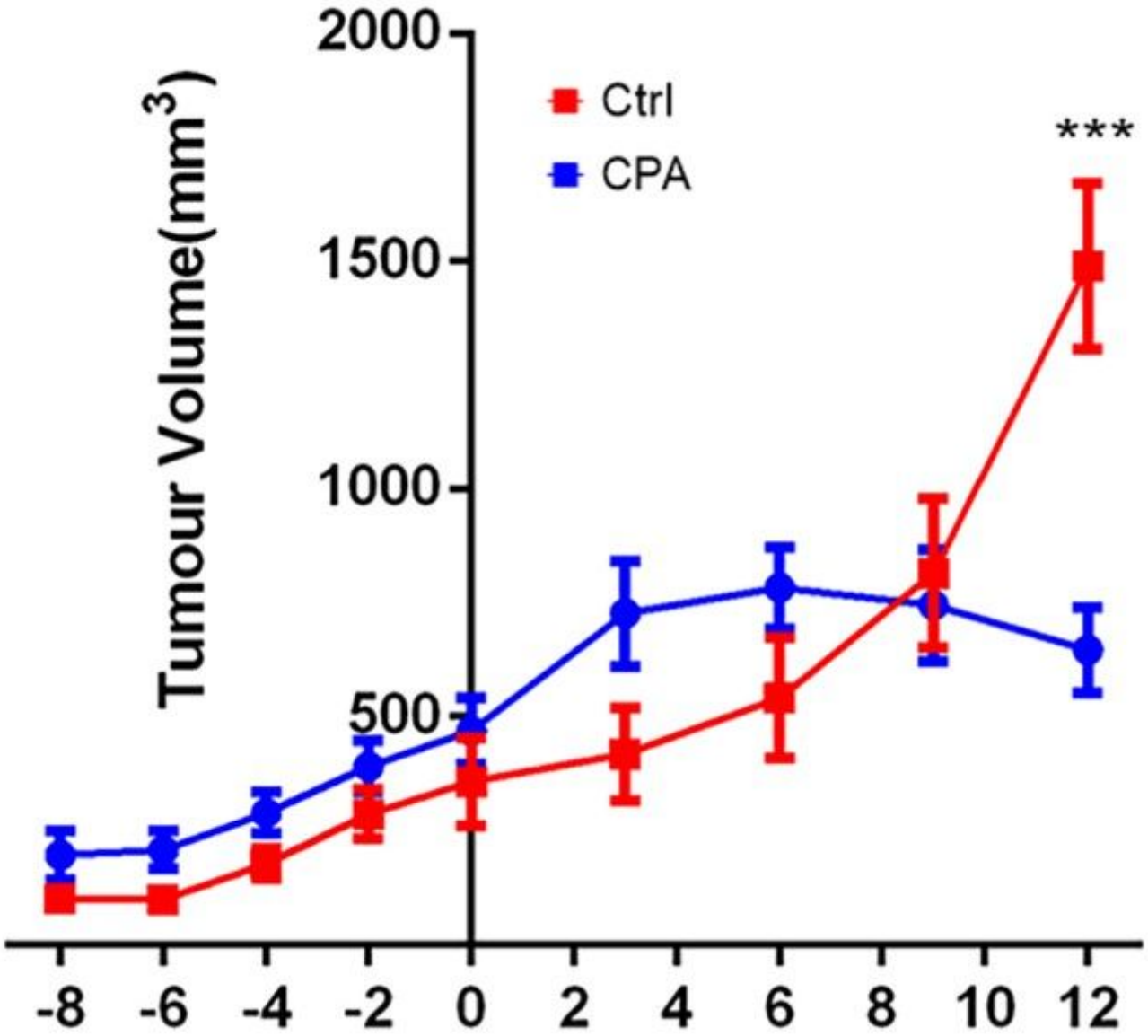

Figure 1

Longitudinal assessment of the tumor volume in the two groups. The data are presented as the mean ± standard deviation. *P < 0.05, **P < 0.01 and ***P < 0.001 refer to comparisons between groups at corresponding time points using the two-independent-samples t-test.

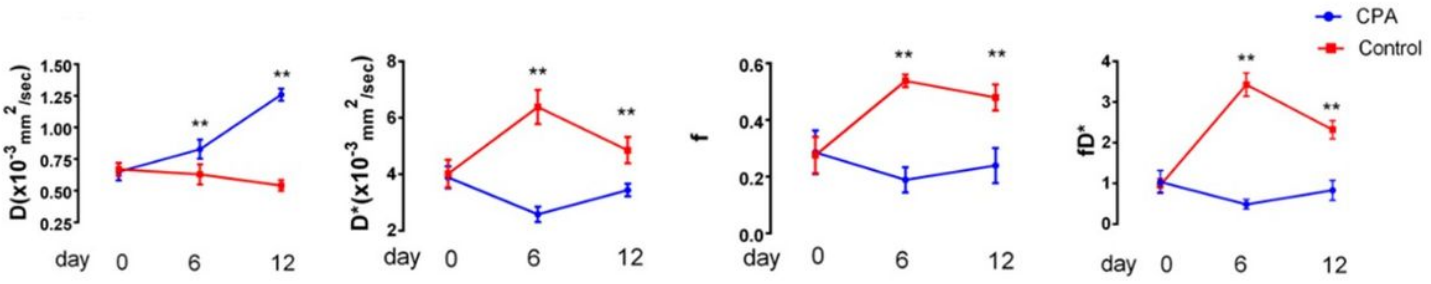

Figure 2

Longitudinal assessments of the MRI parameters in the CPA and control groups. Data points are plotted as medians and ranges. *P < 0.05, **P < 0.01 and ***P < 0.001 refer to comparisons between groups at corresponding time points using the Wilcoxon rank-sum test.

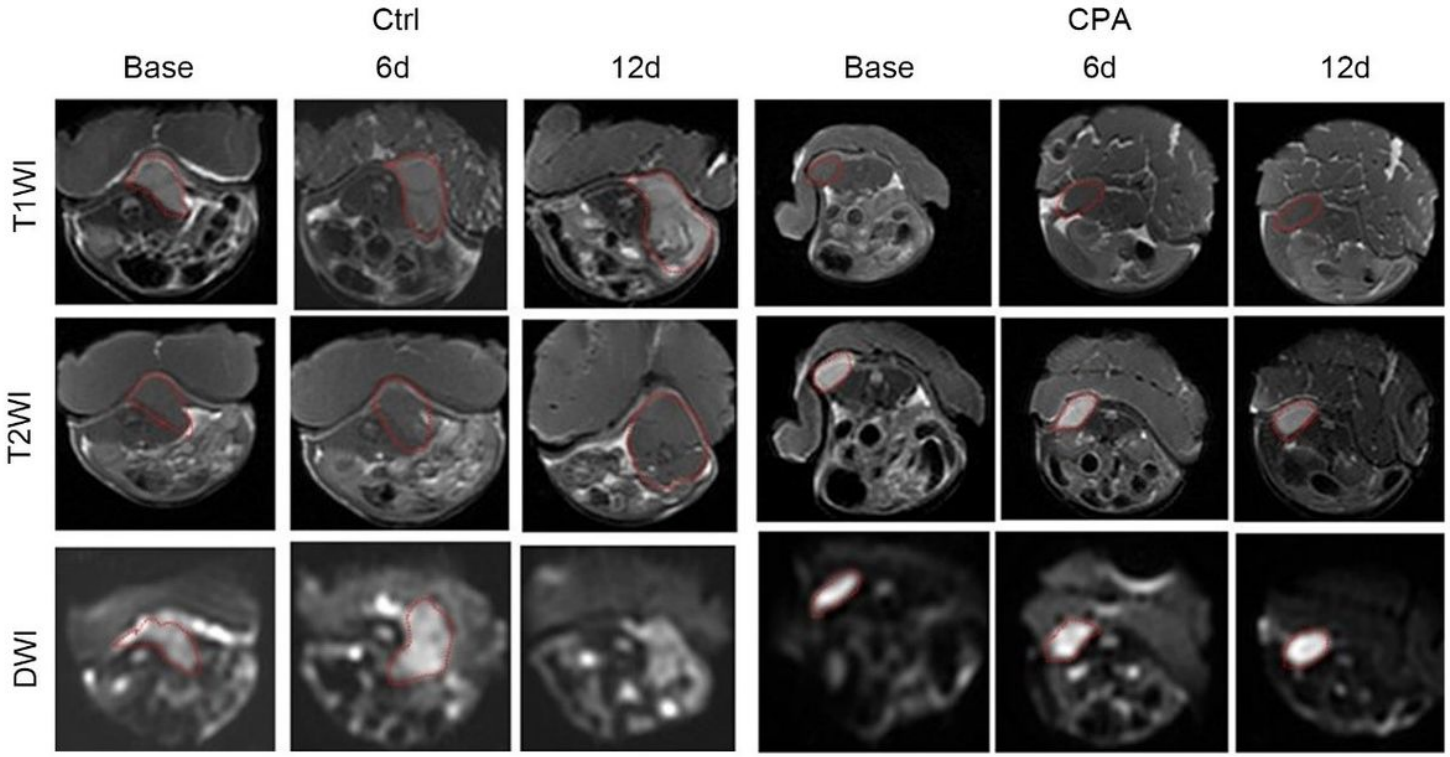

Figure 3

Conventional MRI (T1- and T2-weighted images) and functional maps of representative tumors in mice before and at different time points, after treatment in the control and CPA-treated groups. Dashed outlines denote tumor areas.

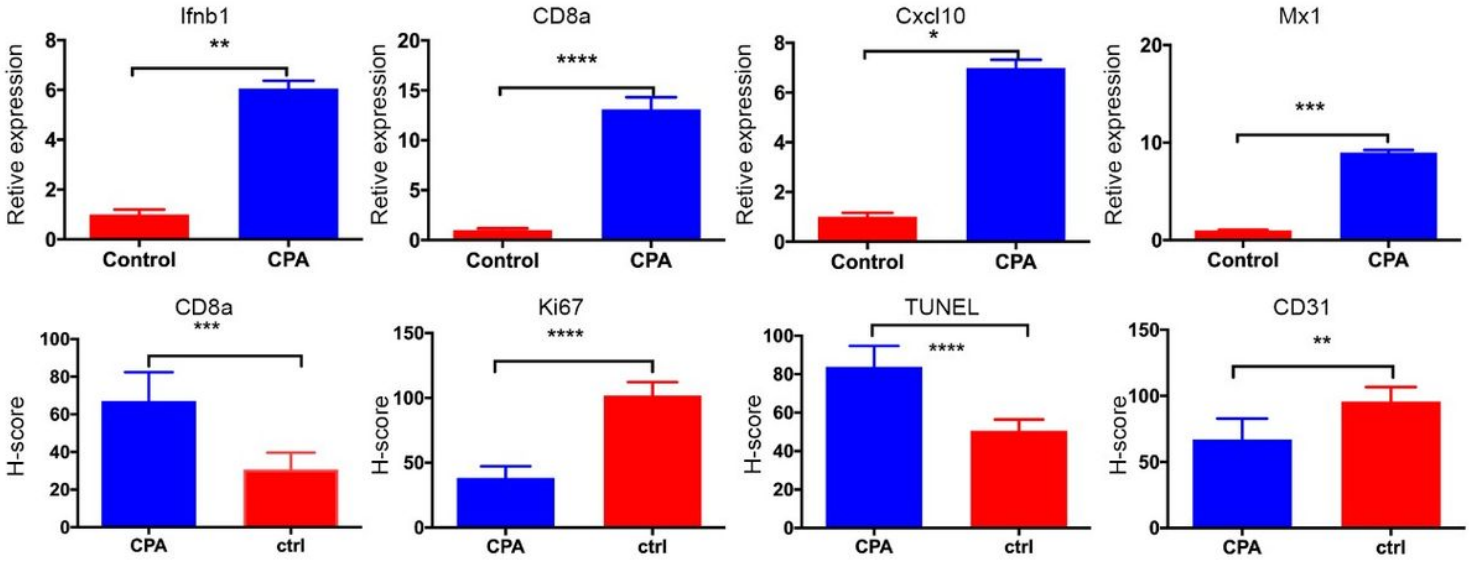

Figure 4

Quantitative results of pathological indicators in the CPA and control groups. The data are presented as the mean ± standard deviation. *P < 0.05, **P < 0.01 and ***P < 0.001 refer to comparisons between groups on day 12 using the two-independent-samples t-test.

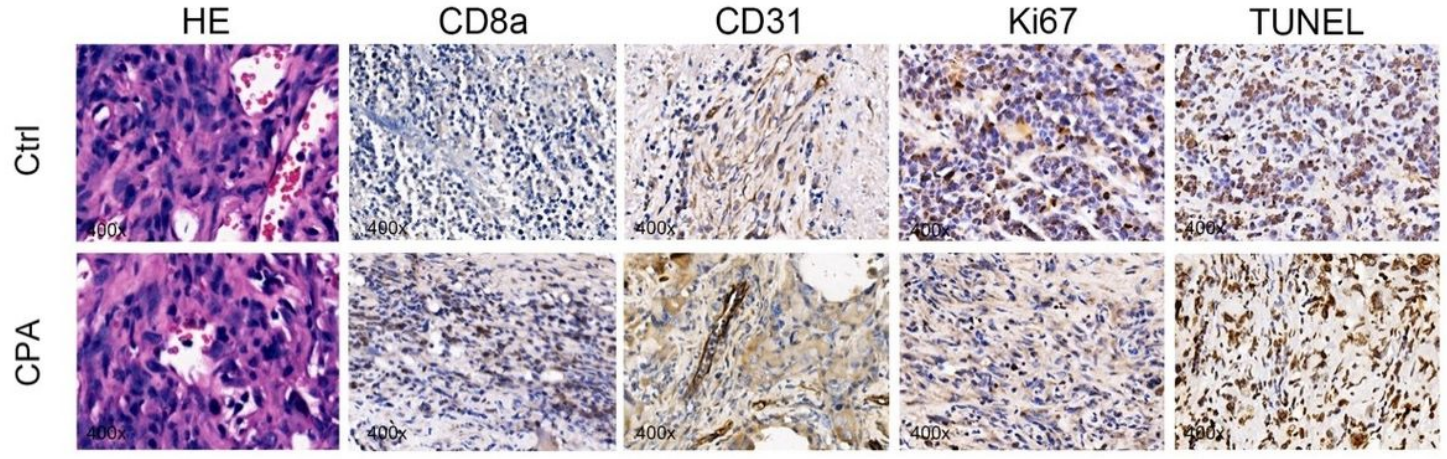

Figure 5

Representative pictures of HE (×400), CD8a (×400), CD31 (×400), Ki67 (×400), and TUNEL staining (×400) between groups on day 12 after treatment.

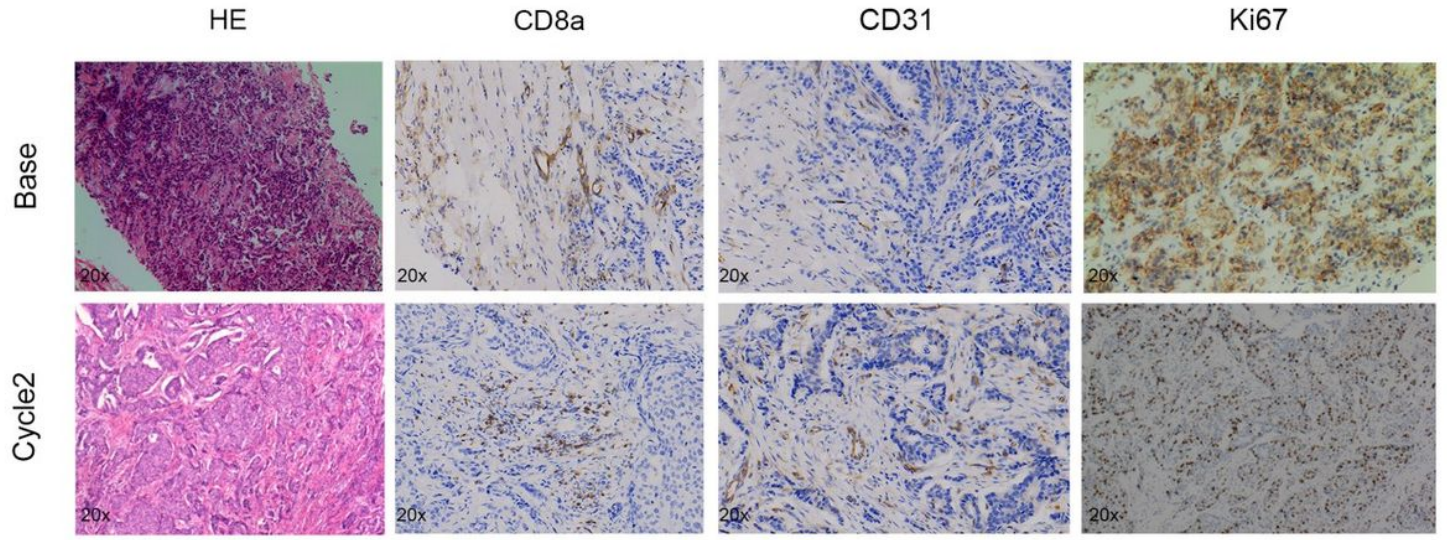

Figure 6

Pathologic tumor changes after neoadjuvant chemotherapy treatment in breast cancer. Representative HE (×20), CD8a (×20), CD31 (×20), and Ki67 (×20) at baseline and time points after 2 cycles of treatment.

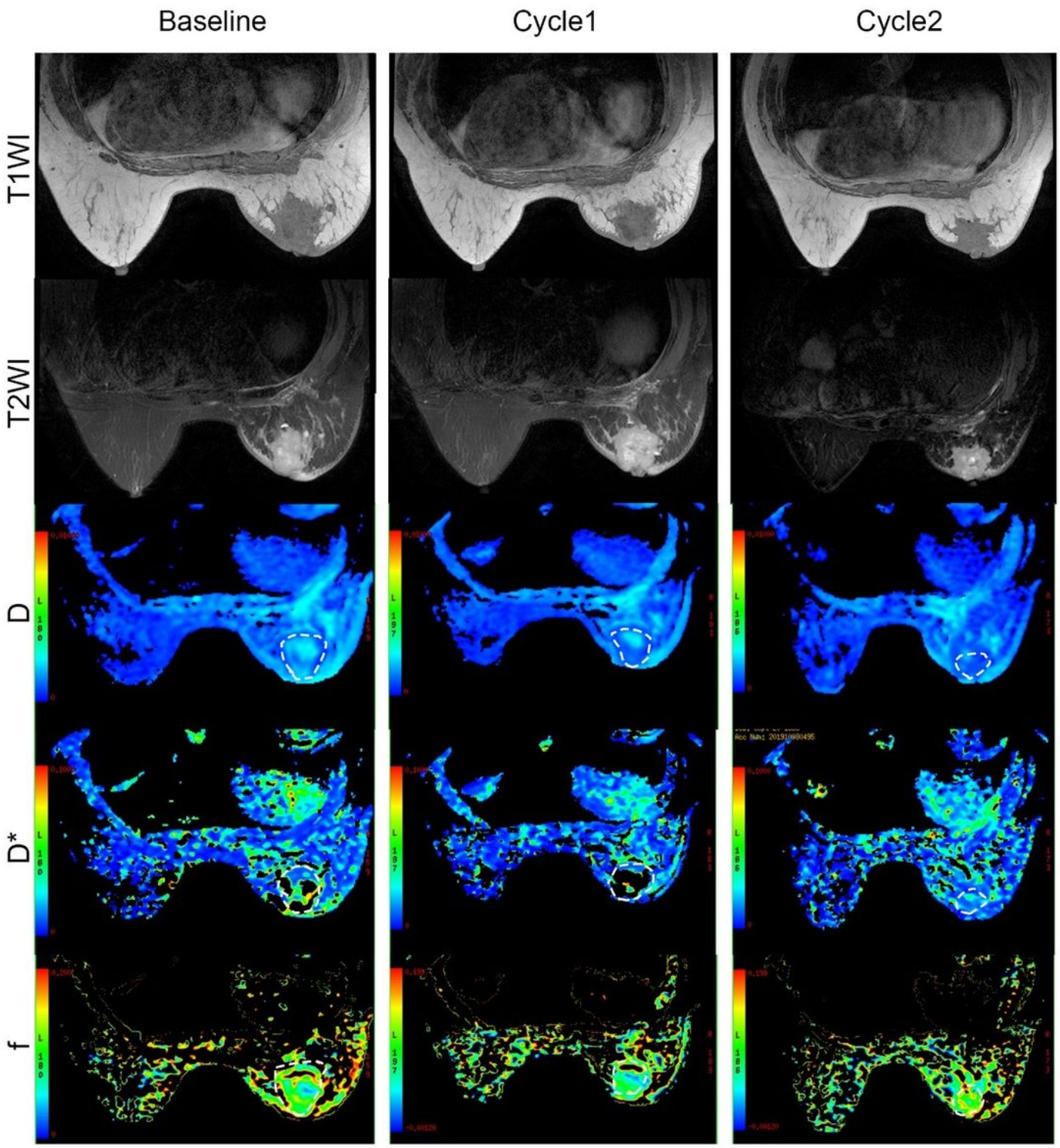

Figure 7

Conventional MRI (T1- and T2-weighted images) and functional maps in breast cancer patients with 2 cycles of immunochemotherapy. Dashed outlines denote tumor areas. Color ranging from blue to red represents values ranging from low to high.

Supplementary Files

This is a list of supplementary files associated with this preprint. Click to download.

- Table1and2.docx